Food Science WILEY

Heat transfer analysis during hydrothermal treatment of mango

Bibiane Pierre-Noel-Gilles[1] | **Rosalina Iribe-Salazar[1]** | **Yessica Vázquez-López[2]** | **José Caro-Corrales[1]** (ID)

[1] Posgrado en Ciencia y Tecnología de Alimentos, Facultad de Ciencias Químico Biológicas, Universidad Autónoma de Sinaloa, Calzada de las Américas Nte 2771, Burócrata, Culiacán, Sinaloa 80013, México

[2] Posgrado en Ciencias Agropecuarias, Facultad de Medicina Veterinaria y Zootecnia, Universidad Autónoma de Sinaloa, Boulevard San Ángel, Fraccionamiento San Benito 3886, Culiacán, Sinaloa 80260, México

Correspondence
José Caro-Corrales, Posgrado en Ciencia y Tecnología de Alimentos, Universidad Autónoma de Sinaloa, Apdo. Postal 1354, C.P. 80000, Culiacán, Sinaloa, México.
Email: josecaro@uas.edu.mx

Abstract: To export Mexican mango fruit, it is required to comply with phytosanitary regulations, which implies heat transfer. Foods are biological systems with a dynamic behavior and, when they are thermally processed, their thermophysical properties change with temperature. Suitable simulation of heat transfer with temperature-dependent thermophysical properties can provide proper estimations of temperature histories to perform heat penetration analyses. The objective of this study was to predict temperatures within mango and immersion times by varying the mass of the fruit and water temperature during hydrothermal treatments. Thermal conductivity, specific heat capacity, and apparent density of "Kent" mango peel and pulp were determined. Finite element analysis was used to simulate heat transfer within the mango. Thermal conductivity and density were different for peel and pulp, but thermal diffusivity for both materials was not different. Predicted temperature histories adjusted properly to experimental data throughout the heating process. This indicates that thermophysical properties as a function of temperature for mango peel and pulp, the convective coefficient, the finite element model, and the methodology used to perform the estimations can be useful in the design of hydrothermal treatments for mango.

KEYWORDS
heat transfer, mango, simulation, thermophysical properties

Practical Application: Proper simulation of heat transfer with temperature-dependent thermophysical properties during hot water treatments for mango can provide accurate temperature histories and profiles that allow the prediction of temperatures within the fruit or immersion times by varying the mass and temperature of the heating medium. This will allow a subsequent heat penetration study to predict larval mortality, facilitating the design of quarantine treatments.

1 | INTRODUCTION

The attractive color, unique flavor, and nutritional value of mango make it one of the most widely consumed tropical fruits (Sulistyawati et al., 2020). Mexico is the world's leading mango exporter (Food and Agriculture Organization of the United Nations, 2020); the US market accounts for more than 80% of Mexican exports. The fundamental problem for producers is that mango is a host for various species of fruit flies. In Mexico, an integrated management against fruit flies is applied, the phytosanitary export regulations require postharvest heat treatments for insect pests, established by the United States Department of Agriculture (Hernández et al., 2018). Hot water treatment (HWT) is the most common quarantine procedure used by the mango industry to satisfy those requirements for treatment of most mangoes exported to the United States (Ngamchuachit et al., 2014; Talcott et al., 2005).

HWT for mango is a non-steady state heat transfer process in which both resistances, external (convection) and internal (conduction), are relevant. There are analytical solutions for regular geometries, governed by the Fourier field equation for simulating these processes. These analytical solutions assume constant thermophysical properties. However, for simulating HWT of fruit with irregular geometry, as mango, there are no analytical solutions that allow studies of heat transfer during the process. Since foods are biological systems, when they are thermally processed show a dynamic behavior and their properties change with temperature and time.

The thermophysical properties depend to a great extent on temperature and composition of the food (Iribe-Salazar et al., 2015) and are essential to design any food engineering process, specifically for transformations that include heat transfer (Muramatsu et al., 2017). They are also important for the prediction and control of various changes that occur in foods during thermal processing and storage.

Precise simulation of heat transfer during food processing requires proper knowledge of the food thermophysical properties and boundary conditions. The most important external variable to determine the evolution of a heating/cooling process is the convective heat transfer coefficient. Once the thermophysical properties and the convective coefficient have been determined, the heat transfer within the fruit can be simulated to predict temperature histories (Cronin et al., 2010). Validation of these predictions can be done later by comparison with experimental data.

Finite element analysis (FEA) has been used to successfully simulate various processing operations and specifically heat transfer in a variety of food products (Lau et al., 2017). FEA is useful when the thermophysical properties are position and temperature dependent, the food has an irregular geometry, or the boundary conditions are not linear (Dhalsamant, 2021). There is a great potential in using FEA during food processing to optimize food quality. Mango has an irregular geometry, and it is feasible to simulate the non-steady state heat transfer within the mango using a 3D finite element model with temperature-dependent properties. A proper simulation of heat transfer within the mango can provide information to estimate temperature histories and a further heat penetration analysis. Therefore, it is convenient to simulate heat transfer processes to predict temperature profiles and histories within foods of irregular shape, which can help to achieve optimal conditions that minimize quality loss in the fruit.

Although the theory of heat transfer is well established, the design, study, and optimization of postharvest heat treatments have sometimes been carried out with intensive and ponderous efforts. In addition, most of the time, the obtained results are only useful for the tested fruit under the studied conditions.

Currently, heat transfer during postharvest thermal processing can be studied numerically using computer simulation models. Researches have been published on the application of the heat transfer theory in quarantine thermal studies; however, such reports have been limited to fruit whose shape resembles a sphere, a geometric shape for which there is an analytical solution, and changes in properties with temperature are not considered.

Finite difference methods are used in much of the simulation studies on non-steady state heat transfer. However, there are some situations in which its application is difficult, particularly when the geometry of the system is complex, the boundary conditions are nonlinear, when the body presents anisotropy, or its properties change with position and temperature (Bazyar & Talebi, 2015). Under these conditions, FEA is one of the best tools for the study of postharvest handling processes of fruits and vegetables in which heat transfer is involved. To increase the versatility in the analysis of hydrothermal treatments, the finite element method can be used to simulate non-steady state heat transfer, considering the convective and internal resistances, and thermophysical properties changing with temperature. Therefore, the objective of this study was to predict temperatures within the mango and immersion times by varying the mass of the fruit and water temperature during hydrothermal treatments. This will contribute to the analysis of different time–temperature conditions during the heating process, facilitating the design of quarantine methods for mangoes. A procedure to achieve accurate

predictions of temperature histories within the fruit during HWTs, together with a heat penetration study, will allow to estimate the lethality of the process and the mortality of fruit fly larvae.

2 | MATERIALS AND METHODS

Mango (*Mangifera indica* L.) cv. Kent used in this study were three-fourths physiologically mature and with export quality. Total soluble solids were 10.1 ± 1.2 °Brix, pulp color parameters were $L^* = 75.8 \pm 2.8$, $a^* = 0.4 \pm 2.7$, $b^* = 53.7 \pm 2.5$, and without physical defects. They meet the minimum acceptable requirements in the regulation for Mexican mango packers (EMEX-SAGARPA-BANCOMEXT/SE, 2005), which states that, for "Kent" mango, total soluble solids should be at least 7.4 °Brix and the pulp should have reached a pale-yellow color without any white portions, this color accentuating around the seed. Fruits were harvested manually at orchards of Aguaruto, Culiacán, Sinaloa, México and were washed, excess water was removed using paper towels, and weighted. Finally, they were stored at 13°C until their use. A proximate analysis was performed according to AOAC International (2012); moisture (925.40), proteins (920.152), fats (920.39), and ashes (940.26).

The thermophysical properties (thermal conductivity [k], specific heat capacity [C_p], and apparent density [ρ]) of mango peel and pulp were measured at 20, 30, 40, and 50°C.

2.1 | Thermophysical properties

2.1.1 | Thermal conductivity

Thermal conductivity was measured with the linear heat source or probe method. Pieces of peel and pulp of mango were skewered side by side on a thermal conductivity probe, taking care to eliminate spaces between the pieces. Thermal conductivity (k) was obtained by regression analysis between temperature (T) and the natural logarithm of time (t):

$$T - T_1 = \frac{Q_L}{4\pi k} \ln\left(\frac{t}{t_1}\right) \tag{1}$$

where $Q_L = I^2 R / L$ is the input heat per unit length of the linear source (W/m), I is the supplied current intensity (A), R is the resistance (Ω), and L the length (m) of the probe. The coordinates ($\ln t_1$, T_1) correspond to the instant when the graph of temperature against the natural logarithm of time becomes linear. Six replicates were made for each temperature and part of the fruit (peel and pulp).

2.1.2 | Specific heat capacity

A differential scanning calorimeter (DSC TA Instruments, 2920, New Castle, DE, USA) was used to measure specific heat capacity (C_p). The sample size (m) was approximately 20 mg and the temperature scan rate (dT/dt) was 20°C/min. Hermetically sealed pans were employed and an empty pan was used as a reference (Iribe-Salazar et al., 2015; Kweon et al., 2017). The specific heat capacity was measured from 20 to 50°C. The enthalpy change, ΔH is given on the DSC curve of heat flow against temperature by the difference in heat flow between the baseline and test material curve (Sánchez-Romero et al., 2021). The specific heat capacity can be obtained from:

$$C_P = \frac{E}{dt/dT} \frac{\Delta H}{m} \tag{2}$$

where the calibration constant, E was obtained using a calibrating reference (sapphire) at the temperature of interest (Zhu et al., 2018). Three replicates were performed for each part of the fruit.

2.1.3 | Apparent density

The liquid displacement method was applied to measure the apparent density (ρ), using distilled water as the liquid medium (Iribe-Salazar et al., 2015). For each determination, the mass of the sample was determined using a balance (AND FX-200, A&D Company Limited, Japan). For the determination of the volume, several strips of mango peel and pulp were coated with a thin plastic film and equilibrated at 20, 30, 40, and 50°C. Once the film was removed, the volume displaced by the sample was measured and the density was calculated as the mass–volume ratio. Ten replicates were made for each temperature and part of the fruit. In addition, for estimating apparent density from a correlation, total soluble solids were determined according to AOAC International (2012); a refractometer (300001, Sper Scientific) was used and drops of the pulp extract were placed in the prism. The results were expressed in °Brix.

FIGURE 1   Mango-shaped aluminum body

FIGURE 2   "Kent" mango and thermocouples

2.1.4 | Thermal diffusivity

Based on its definition, the thermal diffusivity (α) was calculated from:

$$\alpha = \frac{k}{\rho C_P} \tag{3}$$

where k, ρ, and C_p are thermal conductivity, density, and specific heat capacity of mango.

2.2 | Convective heat transfer coefficient

For hot water forced convection treatment of mango with water flowing at around 0.2 m/s, the convective heat transfer coefficient (h) was evaluated using the temperature history method. A mango-shaped aluminum body was constructed (Figure 1), a T-type thermocouple was inserted at a depth of 2.8 cm to obtain the experimental temperature histories using a data acquisition system (DAQ, OMB-DAQ-56, Omega Engineering, Stamford, CT, USA). The finite element method was used to obtain the estimated temperature history. The convective coefficient that provided the best fit to the experimental temperature history was tested. The thermophysical properties used for aluminum were thermal conductivity (238 W/m·K), specific heat capacity (908.5 J/kg·K), and density (2701 kg/m^3), respectively (Kaye & Laby, 2019). Fourteen replicates were made.

2.3 | Water heating of mango

The experimental temperature histories during the hydrothermal heating for "Kent" mango were obtained by inserting T-type thermocouples (Figure 2) at 1.6, 2.3, 3.1, and 4.6 cm depth. The last location corresponded to the cold spot, at the pulp–seed border. Once the temperature
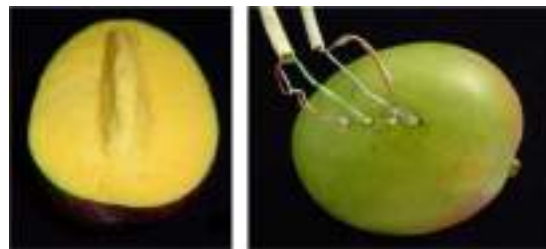
of the cold spot was equilibrated at 21 ± 0.7°C (T_0), fruits were immersed in a water bath at 46 ± 0.5°C (T_∞) for 90 min. The experimental temperature histories for each thermocouple were recorded using a data acquisition system (DAQ, OMB-DAQ-56, Omega Engineering, Stamford, CT, USA).

2.4 | Heat transfer simulation

Heat transfer simulation and predictions were performed by means of the ANSYS software (ANSYS 14.0, Irvine, CA, USA). The dimensions of the 3D model corresponded to a mango of 712 g considering peel and pulp. To simulate heat transfer by conduction, the thermophysical properties were used as a function of temperature for both peel and pulp. The initial temperature, convective coefficient, and water temperature (46°C) were input. Elements were selected from the tetrahedral thermal solid family of ANSYS with 10 nodes, for peel and pulp (Fan et al., 2021). The heat transfer simulation was run for 5400 s and the time step size was 60 s. The validation of simulation during hydrothermal heating of mango was performed by contrasting temperature histories obtained with the finite element solutions to experimental data. To obtain the dip time necessary to reach a selected temperature (43.3°C) at the pulp–seed border, the finite element simulation was accomplished varying water temperature at 47.2, 48.2, and 49.2°C.

2.5 | Experimental design

A completely randomized design was used to evaluate the effect of temperature on the thermophysical properties (k, C_p, ρ, and α) of mango peel and pulp. Factors were temperature (20, 30, 40, and 50°C) and part of the fruit (peel and pulp). Six, three, ten, and three replicates were used for k, C_p, ρ, and α, respectively. Fisher's test was used to compare means ($\alpha = 0.05$).

TABLE 1 Proximate analysis for "Kent" mango at physiological maturity

Composition (g)	Peel	Pulp
Water	72.0 ± 1.39	81.6 ± 3.74
Protein	1.1 ± 0.07	0.7 ± 0.04
Fat	0.4 ± 0.03	0.1 ± 0.01
Ash	1.0 ± 0.07	0.3 ± 0.01
Carbohydrates	25.5	17.3

Note: 100 g of fresh fruit. Total carbohydrates by difference, $n = 4$.

3 | RESULTS AND DISCUSSION

The proximate analysis results of mango peel and pulp at physiological maturity are summarized in Table 1. Moisture, protein, and fat content for peel of "Kent" mango were 72.0 ± 1.39, 1.1 ± 0.07, and 0.4 ± 0.03 g/100 g fresh fruit, respectively. The correspondent variables for pulp of "Kent" mango were 81.6 ± 3.74, 0.7 ± 0.04, and 0.1 ± 0.01 g/100 g fresh fruit. Protein and fat of "Kent" mango pulp in dry basis were 3.80% and 0.54%, respectively. Peel had lower moisture content and higher protein and fat content than pulp, which is consistent with reports by Lago-Vanzela et al. (2011). Likewise, peel showed a higher proportion of ashes and carbohydrates. The proximate composition of "Kent" mango pulp at physiological maturity is similar to the average composition reported by Bernal et al. (2014) for pulp.

3.1 | Thermophysical properties

3.1.1 | Thermal conductivity

Thermal conductivity at 20, 30, 40, and 50°C for peel was 0.587, 0.607, 0.646, and 0.695 W/m·K; while for pulp was 0.614, 0.623, 0.682, and 0.721 W/m·K, respectively. The least significant difference for thermal conductivity was LSD = 0.022 W/m·K. This property was affected ($p < 0.05$) by temperature for peel and pulp and showed a linear increase with temperature. Iribe-Salazar et al. (2015) reported a similar effect of temperature on the thermal conductivity determined with the same method.

The result obtained for peel (0.587 W/m·K) at 20°C is similar to that reported by other authors for foods with similar moisture content (Rahman, 2009). In the case of pulp, thermal conductivity (0.614 W/m·K) at 20°C is 8% higher than that reported by Rahman (2009) for conductivity of carrot (28°C), a material with slightly higher moisture content (90%) than mango pulp.

On the other hand, thermal conductivity estimated at 20°C with Sweat's (1974) correlation for fruits and vegetables was 0.503 and 0.550 W/m·K for peel and pulp, respectively; they were 14.3% and 10.4% lower. This confirms the importance of experimentally evaluating thermophysical properties, since the approximate margin of error for the correlation, indicated by Sweat (1974), is 15%. A relatively high percentage, due to the importance of thermal conductivity in the heat transfer process. In addition, linear equations are proposed to predict thermal conductivity of peel and pulp for "Kent" mango in the range from 20 to 50°C:

$$k_{\text{peel}} = 3.646 \times 10^{-3}T + 0.5061R^2 \tag{4}$$

$$= 0.95, \text{ RMSE} = 0.011\frac{\text{W}}{\text{m.k}}$$

$$k_{\text{pulp}} = 3.825 \times 10^{-3}T + 0.5262R^2 \tag{5}$$

$$= 0.91, \text{ RMSE} = 0.015\frac{\text{W}}{\text{m.k}}$$

Thermal conductivity of pulp was higher than that of peel, which can be explained by the higher moisture content of pulp (9.6% higher) than that for peel; this difference is not proportional since the other components of the food also contribute to its thermal conductivity. As thermal conductivity of peel was lower for the studied temperatures, this indicates that at steady state, heat transfer is slower in peel than in pulp.

3.1.2 | Specific heat capacity

The specific heat capacity for peel, at 20, 30, 40, and 50°C was 2279, 2684, 2738, and 2891 J/kg·K and for pulp, it was 2589, 3049, 3115, and 3368 J/kg·K, respectively. The least significant difference was LSD = 1386 J/kg·K. This property was not affected ($p > 0.05$) by temperature in the studied range. This may be due to heterogeneity in tissue or sample size.

In addition, specific heat capacity of mango peel and pulp was estimated with correlations. Using Alvarado's correlation (Alvarado, 1991), these properties were 3080 and 3372 J/kg·K and using Choi and Okos' correlation (Choi & Okos, 1986), they were 3431 and 3692 J/kg·K, respectively. When comparing these estimations with the mean (there were no differences) for peel (2648 J/kg·K) and pulp (3031 J/kg·K), then Alvarado's correlation estimates a specific heat capacity 16.3% and 11.3% higher and Choi and Okos' correlation 29.6% and 21.8% higher for peel and pulp, respectively. This may be because these correlations were developed for a wide range of foods with diverse moisture, fat, protein, and carbohydrate content.

3.1.3 | Apparent density

Density at 20, 30, 40, and 50°C was 1081, 1101, 1115, and 1135 kg/m^3, for peel; and 1034, 1048, 1058, and 1082 kg/m^3

for pulp, respectively. The least significant difference was LSD = 12.3 kg/m^3. Peel had the highest density, since the structure of peel is more compact than that of pulp. On the other hand, temperature affected ($p < 0.05$) density of both peel and pulp in the temperature range.

Density of mango pulp was estimated using Alvarado and Romero's correlations (Alvarado & Romero, 1989). Total soluble solids for pulp were 10.3, 14.2, and 19.5 °Brix at 20, 30, and 50°C, respectively. From correlation that considers only soluble solids, estimated density was 1039, 1055, and 1077 kg/m^3, and from that based on soluble solids and temperature, 1042, 1057, and 1075 kg/m^3. Results indicate that density is similar to that estimated through the correlations; closer to the estimation using the correlation based only on °Brix than that using °Brix-temperature. This effect seems not to be a consequence on temperature increase, but rather on °Brix increase, as denoted by the coefficients in the mathematical expression of the correlations.

3.1.4 | Thermal diffusivity

Thermal diffusivity for peel at 20, 30, 40, and 50 °C for "Kent" mango was 2.40×10^{-7}, 2.03×10^{-7}, 2.13×10^{-7}, and 2.12×10^{-7} m^2/s, while for pulp was 2.32×10^{-7}, 1.95×10^{-7}, 2.10×10^{-7}, and 2.02×10^{-7} m^2/s, respectively. The least significant difference was LSD = 1.54×10^{-8} m^2/s. Thermal diffusivity of peel decreased ($p < 0.05$) from 20 to 30°C, while no effect was obtained at 30, 40, and 50°C. Thermal diffusivity of pulp showed a similar behavior to that of peel, a decrease ($p < 0.05$) from 20 to 30°C, and subsequently a constant behavior from 30 to 50°C.

When comparing thermal diffusivity of peel and pulp, there were no differences ($p > 0.05$) for both parts of the fruit at each temperature, despite there being differences between thermal conductivity and density of peel and pulp. This behavior may be due to the variability obtained for specific heat capacity. However, Martens (1980) found that the variation in the solid fraction of fats, proteins, and carbohydrates showed a minimal influence on thermal diffusivity; therefore, according to Martens (1980), temperature and moisture content are the main factors that show an effect on thermal diffusivity of foods.

3.2 | Heat transfer simulation

The thickness of "Kent" mango peel was 1.7 mm, with a coefficient of variation of 1.01% ($n = 12$). The finite element geometry for mango, created using the pulp dimensions (4.6 cm) of a 712 g mango and the peel thickness is shown in Figure 3. The meshed 3D volume resulted in 9361
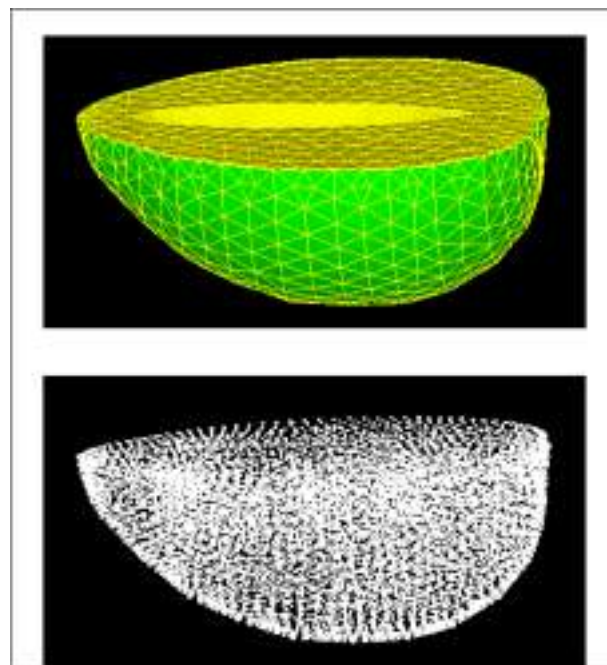

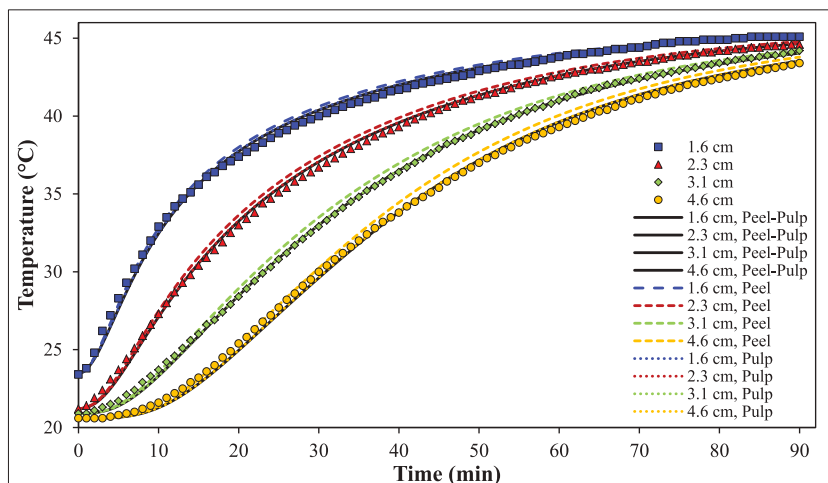**FIGURE 3** Finite element and node geometry of 3D model for mango

elements and 14,111 nodes with an element size less than 1 cm; no improvement was obtained when using an element size of 0.5 cm. This may provide a closer approximation to the dynamic behavior of heat transfer within the mango, which will be confirmed by comparing with experimental data.

To estimate the convective heat transfer coefficient, a regression analysis between the experimental unaccomplished temperature ratio history during heating of the mango-shaped aluminum body and that estimated with the finite element method was performed. The average heat transfer coefficient obtained during the stages of validation and prediction, which provided the best fit ($R^2_{adj} > 0.998$ and 0.989, RMSE $< 9.8 \times 10^{-3}$ and 0.014) under the studied conditions were 1182 and 823 W/m^2 K, and the coefficient of variation was 5.3% and 5.9%, respectively, which is an indicator of a good reproducibility.

3.3 | Temperature histories

Temperature histories simulated through FEA using temperature-dependent properties for mango peel and pulp, and experimental results for validation at depths of 1.6, 2.3, 3.1, and 4.6 cm are shown in Figure 4. Since there were no differences between thermal diffusivity of mango peel and pulp, two new groups of temperature histories were simulated with temperature-dependent properties. The first using the peel properties for both parts of the fruit

FIGURE 4 Temperature histories simulated through finite element analysis using peel, pulp, and peel–pulp properties and experimental results (markers) at depths of 1.6, 2.3, 3.1, and 4.6 cm

and the second with pulp properties for the entire mango (Figure 4).

When different properties are used for peel and pulp, there is a great concordance between the simulated and experimental temperature histories throughout the entire heat transfer process. The high determination coefficients ($R^2 > 0.998$, RMSE < 0.24°C) indicate that temperature histories obtained through FEA fit properly to the experimental results. The highest temperature difference between temperature histories (0.8°C) was obtained for 1.6 cm depth at 3 min of the process. Temperature differences are due to the irregular geometry of the mango and have a special role on the more thermo-sensible zones causing the surface quality may be affected.

When peel or pulp properties are used for the entire mango, the highest temperature difference (0.6°C) occurred at 4.6 cm depth and 34 min of heating when peel properties were used for both parts of the fruit, compared to simulation using peel–pulp properties. This allows confirming that heat transfer modeling can be done without differentiating between properties of peel and pulp.

Figure 5 displays snapshots of the temperature distribution within the mango at different water heating times. High temperature gradients between peel and locations at 2 cm depth are obtained at 5 min of heating. These temperature gradients decrease as the process continues; after 20 min, the temperature difference between pulp and pulp–seed border is almost 20°C, and at 85 min, it is less than 2°C. At this time (85 min of heating), temperature of the entire mango is higher than 43.1°C. Figure 6 displays the evolution of heat flux density within mango at different process times. The highest flux densities (∼4000 W/m²) are obtained at 1 min of heating and are located near the peel. After 5 min of the process, the region near the peduncle shows the highest flux densities. As the process continues, heat flux density decreases since tempera-

TABLE 2 Temperature estimated by finite element at different pulp depths, simulating dip in water at 46°C and 90 min of heating

Depth (cm)	Temperature (°C)	
	Experimental	Finite element
1.6	45.1 ± 0.07	45.1
2.3	44.6 ± 0.06	44.6
3.1	44.2 ± 0.06	44.0
4.6	43.4 ± 0.05	43.5

ture gradients also decrease, and the flux density is appreciable in the region near the pulp–seed border. At 30 min of heating, heat flux density in the apical region is lower than that in the equatorial region, since temperature gradients are around 3°C in the first region and almost 20°C in the latter one. At 20 min of water heating, the highest flux density is around 570 W/m² and at 90 min, it has changed from 2 to 53 W/m² for the entire mango.

Temperature estimated by finite element at different pulp depths, simulating dip in water at 46°C and 90 min of heating and the corresponding experimental results are shown in Table 2. The highest difference (0.2°C) at 90 min was obtained for 3.1 cm depth. Therefore, from results of thermophysical properties as a function of temperature, the convective heat transfer coefficient, and the finite element model, different process conditions can be assayed to get suitable HWTs and subsequent heat penetration analyses.

3.4 | Parameter studies

During water heating of mango, the temperature–time combination depends on the fruit size and the pest to be eliminated; HWTs should allow a rise in fruit heart tem-
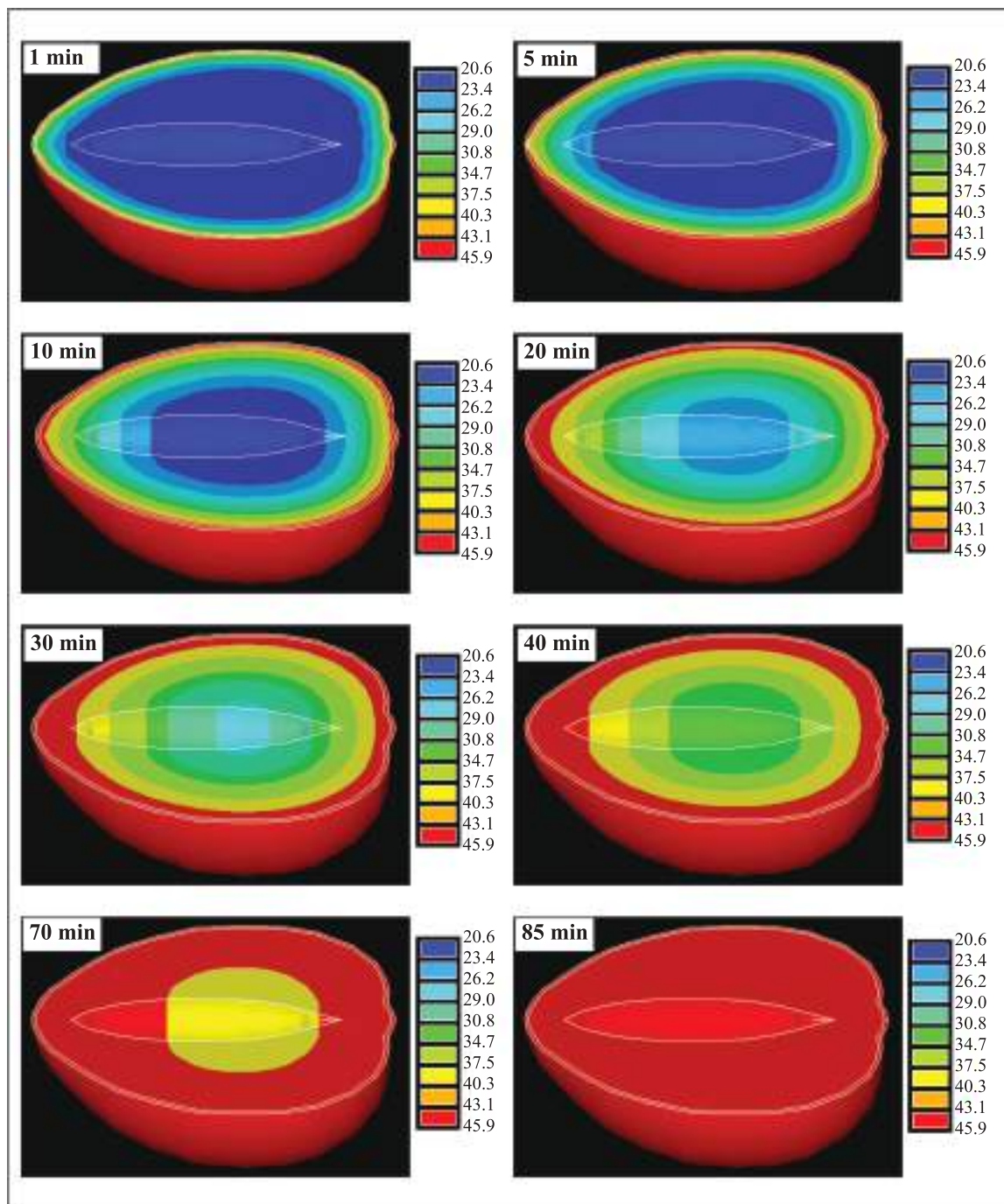
FIGURE 5   Snapshots of ANSYS model temperature distribution for mango. Numbers in legends indicate temperature (°C)

perature varying between 43.3 and 46.7°C (Ducamp-Collin et al., 2007). Therefore, the immersion time for the pulp core to reach 43.3°C should be evaluated. The simulated temperature at dip time to experimentally reach 43.3°C for different pulp depths is shown in Table 3. The highest difference (0.3°C) arises at 1.6 and 2.3 cm depth when peel properties were used for both parts of the fruit. On the other hand, temperature simulated with pulp properties for both sections of mango did not differ from that

estimated with peel and pulp properties for 2.3, 3.1, and 4.3 cm depth. Accordingly, the simulated temperature can be obtained either by using properties for each part of the fruit and by using only those of peel or pulp for the entire mango.

Even though the obtained results were widely satisfactory, a comparison was made of the experimental temperature history for the pulp cold spot (4.6 cm) and three temperature histories estimated with finite element.
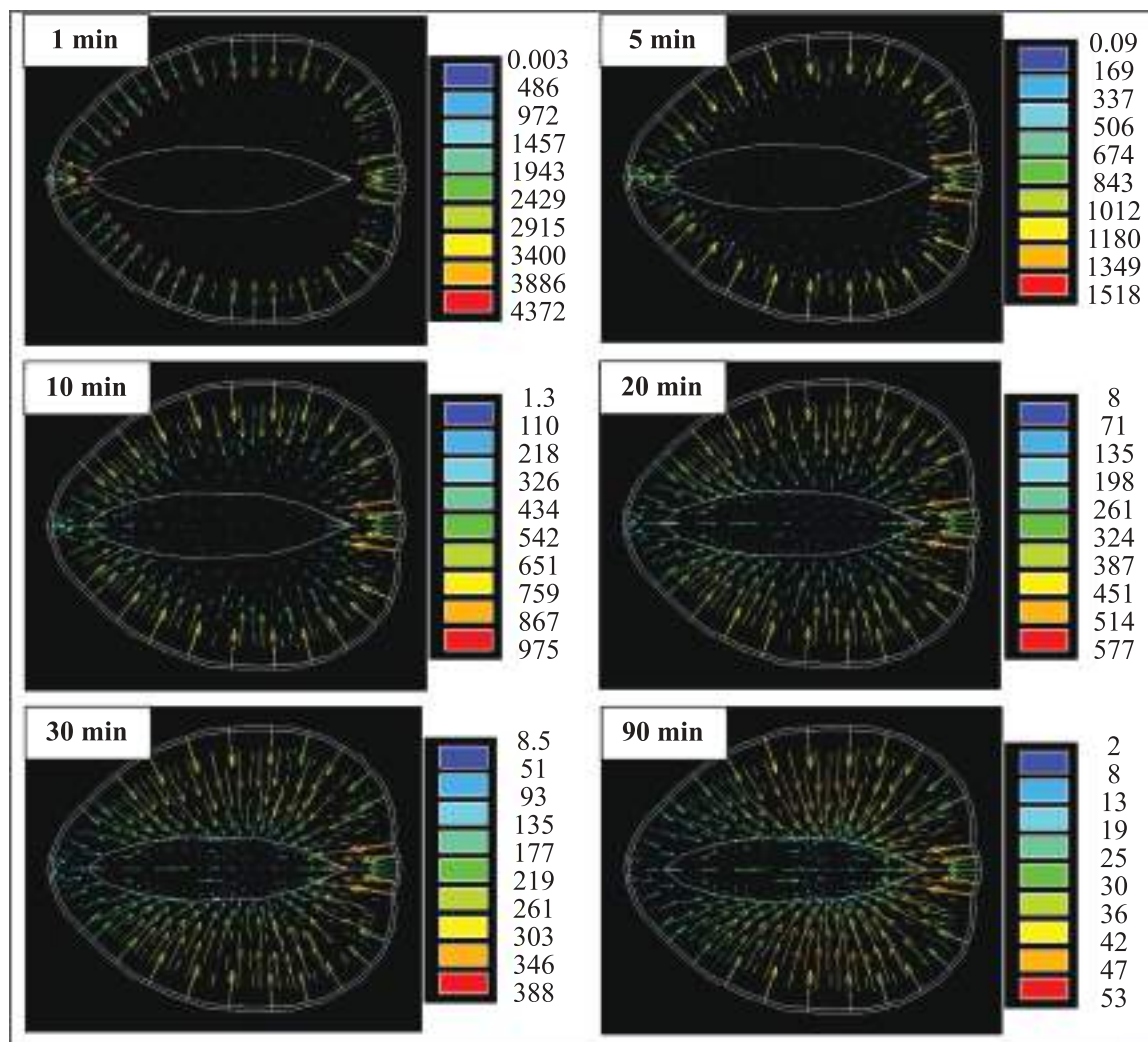
FIGURE 6 Snapshots of ANSYS model heat flux density distribution for mango. Numbers in legends indicate heat flux density (W/m^2)

TABLE 3 Temperature at the dip time to reach 43.3°C for different pulp depths

			Temperature (°C)		
Depth (cm)	Time (min)	Target	Peel–pulp properties	Peel properties	Pulp properties
1.6	54	43.3	43.4	43.6	43.5
2.3	68	43.3	43.4	43.6	43.4
3.1	79	43.3	43.3	43.5	43.3
4.6	89	43.3	43.5	43.7	43.5

The first with properties as a function of temperature (variable properties, VP); the second, assuming constant properties (constant properties, CP) at 20°C; and the third, simulating with the thermal conductivity and specific heat capacity obtained from Sweat's and Alvarado's correlation; and for density, at 20°C (constant properties by correlations, CPC). Temperature histories are shown in Figure 7.

The temperature history that agrees with experimental results, during the entire heat transfer process, is the one generated using temperature-dependent properties. When the simulation is performed with constant properties, the maximum experimental temperature (43.4°C) is reached earlier (13 min), while in the estimation with constant properties obtained by correlations (CPC), the target tem-

TABLE 4   Dip time to reach 43.3°C at the cold spot for different mangoes and water temperature

Category 1						
Mass/g	T_w/°C	T_i/°C	Depth/cm	t_{est}/min	t_{exp}/min	R^2_{adj}
423	47.2	18.4	3.2	59	60	0.996
479	48.2	20.3	3.2	54	54	0.996
479	49.2	20.6	3.5	52	52	0.998
Category 2						
712	47.2	20.5	4.2	76	76	0.996
603	48.2	21.4	3.8	65	65	0.997
528	49.2	21.5	3.8	55	54	0.998
Category 3						
822	47.2	21.0	5.2	88	89	0.998
781	48.2	20.5	4.8	78	78	0.999
770	49.2	22.8	4.7	71	71	0.998

Note: Mass, mango mass (g); T_w, water temperature (°C); T_i, initial temperature (°C); t_{est}, estimated time (min); t_{exp}, experimental time (min).

FIGURE 7   Temperature histories with variable properties (VP), constant properties (CP) at 20°C, and constant properties obtained by correlations (CPC)

perature is not reached at 90 min, but up to 116 min of heating.

The goodness of fit between the estimated and experimental histories was determined comparing the natural logarithm of the unaccomplished temperature ratios. The best fit (R^2_{adj} = 0.9998, RMSE = 0.01) was obtained when properties as a function of temperature (VP) was used. As can be seen from these results, simulating heat transfer using experimentally determined properties and considering the effect of temperature on thermophysical properties, allows to obtain the precision required for the design of HWTs for mango. This procedure can be used to predict temperatures and/or immersion times,

varying the conditions: pulp depths and heating medium temperature.

3.5 | Dip time to reach 43.3°C varying mango mass and water temperature

The predicted and experimental temperature histories are shown in Figures 8–10. These histories show the high agreement throughout the heating process. When validating the predictions, comparing the simulated and experimental temperatures, the lowest R^2_{adj} was 0.995 (RMSE < 0.61), corresponding to 423 g, 3.2 cm depth, from
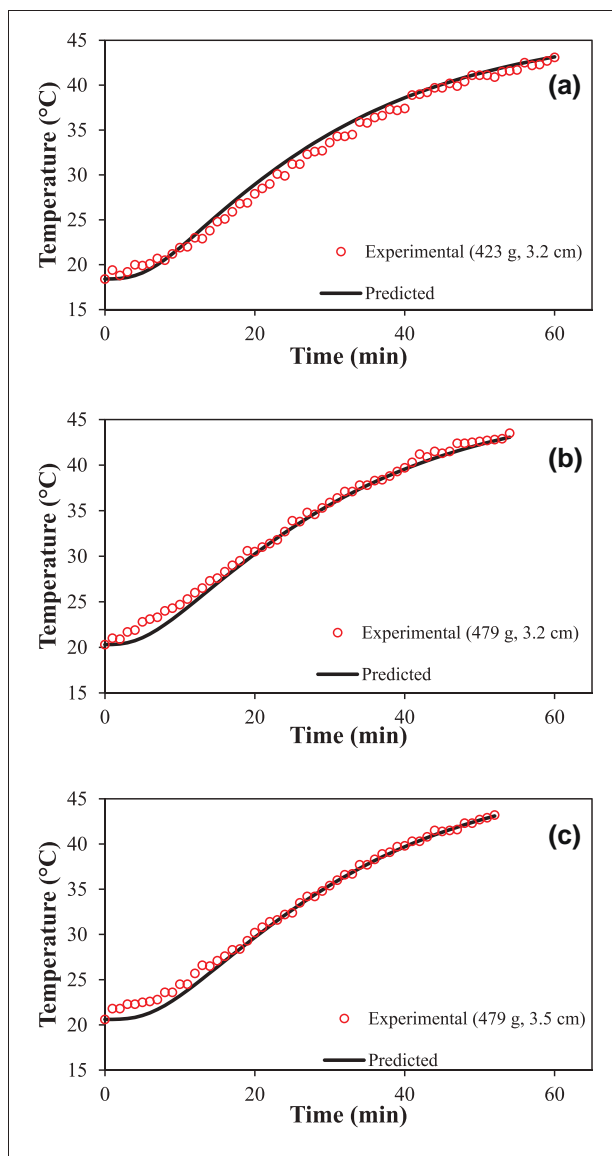
FIGURE 8 Category 1; simulated (—) and experimental (•) temperature histories for mango varying mass and water temperature at 47.2°C (a), 48.2°C (b), and 49.2°C (c)

FIGURE 9 Category 2; simulated (—) and experimental (•) temperature histories for mango varying mass and water temperature at 47.2°C (a), 48.2°C (b), and 49.2°C (c)

category 1; it indicates the high degree of fit obtained when carrying out the simulations. The mass difference between mangoes did not necessarily coincide with the cold spot depth difference. For example, in mango of category 1 the cold spot was located at 3.2 cm for two mangoes with a mass difference of 56 g; the same was obtained for the other two categories. The dip time to reach 43.3°C at the cold spot for different mango mass and water temperature is shown in Table 4. The predicted dip time coincided with the experimental result in most cases and in the rest the difference was less than 1 min. These results indicate that heat transfer simulations through FEA can
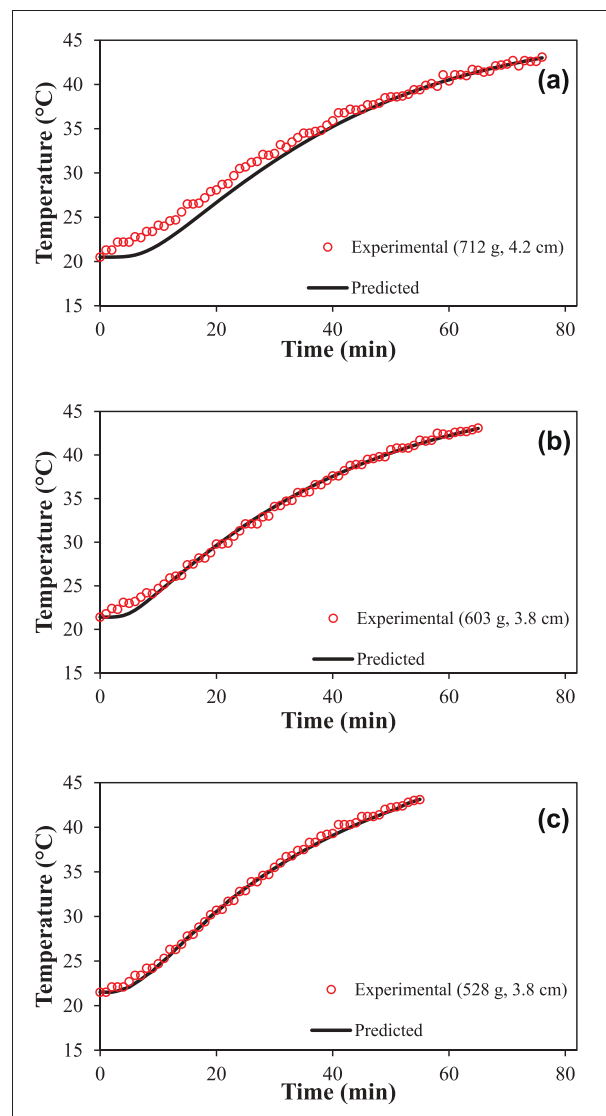
be useful to estimate temperature histories in HWTs for mango.

4 | CONCLUSIONS

Heat transfer simulation can be done using only thermophysical properties of pulp for the entire "Kent" mango, without using peel properties. Performing heat transfer analysis using constant thermophysical properties or those obtained by correlations will not render satisfactory results. Heat transfer analysis considering the effect of temperature on thermophysical properties can allow obtaining the necessary accurate for the design of HWTs for mango.
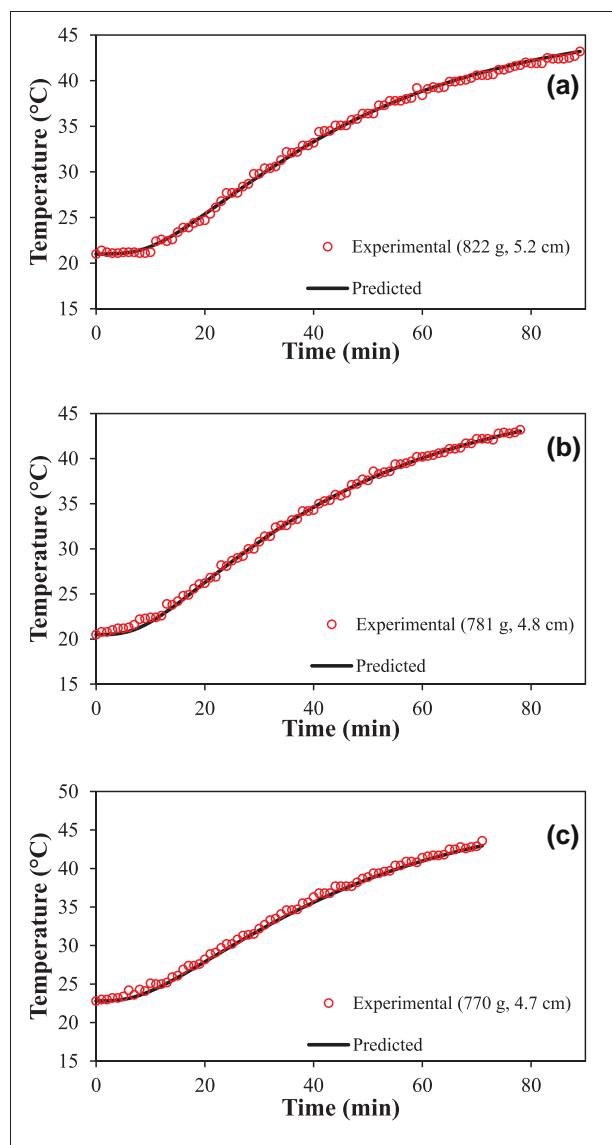
FIGURE 10 Category 3; simulated (—) and experimental (•) temperature histories for mango varying mass and water temperature at 47.2°C (a), 48.2°C (b), and 49.2°C (c)

By varying the mango mass and water temperature, a high agreement ($R^2_{adj} > 0.995$) was obtained between the predicted temperatures within the mango and the experimental ones throughout the hydrothermal treatment. The dip time estimated by FEA, varying the mass of the mango and water temperature, differed in less than 1 min from the experimental times. The results confirmed that thermophysical properties as a function of temperature for mango peel and pulp, the convective coefficient, the 3D model created for the FEA, and the methodology used to perform the estimations can be useful to analyze different water temperature–time conditions for hydrothermal treatments to disinfest mango from immature stages of fruit fly larvae trying to reduce the loss of quality in the fruit.

AUTHOR CONTRIBUTIONS

Bibiane Pierre-Noel-Gilles: Conceptualization; data curation; formal analysis; investigation; methodology; validation. **Rosalina Iribe-Salazar**: Conceptualization; data curation; formal analysis; investigation; validation; visualization; writing – original draft; writing – review and editing. **Yessica Vázquez-López**: Conceptualization; data curation; formal analysis; investigation; validation; visualization; writing – original draft; writing – review and editing. **José Caro-Corrales**: Conceptualization; data curation; formal analysis; investigation; methodology; project administration; resources; supervision; validation; visualization; writing – original draft; writing – review and editing.

ORCID
José Caro-Corrales https://orcid.org/0000-0003-1496-0507

REFERENCES

Alvarado, J. D. D. (1991). Specific heat of dehydrated pulps of fruits. *Journal of Food Process Engineering*, *14*(3), 189–196. https://doi.org/10.1111/j.1745-4530.1991.tb00090.x

Alvarado, J. D. D., & Romero, C. H. (1989). Physical properties of fruits: I – Density and viscosity of juices as functions of soluble solids content and temperature. *Latin American Applied Research*, *19*(15), 15–21.

AOAC International. (2012). *Official methods of analysis of AOAC international* (19th ed.) AOAC International.

Bazyar, M. H., & Talebi, A. (2015). Scaled boundary finite-element method for solving non-homogeneous anisotropic heat conduction problems. *Applied Mathematical Modelling*, *39*, 7583–7599. https://doi.org/10.1016/j.apm.2015.03.024

Bernal, A., Maldonado, M., Urango, L., Franco, M., & Rojano, B. (2014). Mango de azúcar (*Mangifera indica*), variedad de Colombia: Características antioxidantes, nutricionales y sensoriales. *Revista Chilena de Nutrición*, *41*, 312–318. https://doi.org/10.4067/S0717-75182014000300013

Choi, Y., & Okos, M. R. (1986). Effects of temperature and composition on the thermal properties of foods. In L. M. Maguer & P. Jelen (Eds.), *Food engineering and process applications: Transport phenomena* (Vol. 1, pp. 93–101). Elsevier.

Cronin, K., Caro-Corrales, J., & Gao, X. (2010). Heat transfer analysis of cheese cooling incorporating uncertainty in temperature measurement locations: Model development and validation. *Journal of Food Engineering*, *99*, 175–183. https://doi.org/10.1016/j.jfoodeng.2010.02.016

Dhalsamant, K. (2021). Development, validation, and comparison of FE modeling and ANN model for mixed-mode solar drying of potato cylinders. *Journal of Food Science*, *86*, 3384–3402. https://doi.org/10.1111/1750-3841.15847

Ducamp Collin, M. N., Arnaud, C., Kagy, V., & Didier, C. (2007). Fruit flies: Disinfestation, techniques used, possible application to mango. *Fruits*, *62*(4), 223–236. https://doi.org/10.1051/fruits:2007018

EMEX-SAGARPA-BANCOMEXT/SE. (2005). Empacadoras de Mango de Exportación /Secretaría de Agricultura, Ganadería, Desarrollo Rural, Pesca y Alimentación/Banco de Comercio Exterior/Secretaría de Economía. PC-005-2005 Pliego de Condiciones para el uso de la Marca Oficial México Calidad Suprema en Mango. México City, p. 33. https://www.siar.mx/file/files/Mexico%20Calidad%20Suprema/Mango.pdf

Fan, H., Huang, J., Zhao, J., Yan, B., Ma, S., Zhou, W., Zhang, H., & Fan, D. (2021). Electromagnetic properties of crayfish and its responses of temperature and moisture under microwave field. *Journal of Food Science*, *86*(4), 1306–1321. https://doi.org/10.1111/1750-3841.15667

Food and Agriculture Organization of the United Nations. (2020). *FAOSTAT statistical database.* http://www.fao.org/faostat/es/#data/QC.

Hernández, E., Aceituno-Medina, M., Toledo, J., Gómez-Simuta, Y., Villarreal-Fuentes, J. M., Carrasco, M., & Montoya, P. (2018). Generic irradiation and hot water phytosanitary treatments for mango fruits *cv.* 'Ataulfo' niño infested by *Anastrepha ludens* and *Anastrepha obliqua* (Diptera: Tephritidae). *Journal of Economic Entomology*, *111*(5), 2110–2119. https://doi.org/10.1093/jee/toy198

Iribe-Salazar, R., Caro-Corrales, J., Hernández-Calderón, Ó., Zazueta-Niebla, J., Gutiérrez-Dorado, R., Carrazco-Escalante, M., & Vázquez-López, Y. (2015). Heat transfer during blanching and hydrocooling of broccoli florets. *Journal of Food Science*, *80*, E2774–E2781. https://doi.org/10.1111/1750-3841.13109

Kaye, G. W. C., & Laby, T. H. (2019). Tables of Physical and Chemical Constants and Some Mathematical Functions. Alpha Editions. 164.

Kweon, M., Slade, L., & Levine, H. (2017). Differential scanning calorimetry analysis of the effects of heat and pressure on protein denaturation in soy flour mixed with various types of plasticizers. *Journal of Food Science*, *82*(2), 314–323. https://doi.org/10.1111/1750-3841.13616

Lago-Vanzela, E., Ramin, P., Guez, M. A. U., Santos, G., Gomes, E., & Da Silva, R. (2011). Chemical and sensory characteristics of pulp and peel 'cajá-manga' (*Spondias cytherea* Sonn.) jelly. *Food Science and Technology*, *31*, 398–405. https://doi.org/10.1590/S0101-20612011000200018

Lau, S. K., Thippareddi, H., & Subbiah, J. (2017). Radiofrequency heating for enhancing microbial safety of shell eggs immersed in deionized water. *Journal of Food Science*, *82*, 2933–2943. https://doi.org/10.1111/1750-3841.13965

Martens, T. (1980). *Mathematical model of heat processing in flat containers* [Ph.D. thesis, Katholeike University, Leuven, Belgium].

Muramatsu, Y., Greiby, I., Mishra, D. K., & Dolan, K. D. (2017). Rapid inverse method to measure thermal diffusivity of low-moisture foods. *Journal of Food Science*, *82*, 420–428. https://doi.org/10.1111/1750-3841.13563

Ngamchuachit, P., Barrett, D. M., & Mitcham, E. J. (2014). Effects of 1-methylcyclopropene and hot water quarantine treatment on quality of "Keitt" mangos. *Journal of Food Science*, *79*, C505–C509. https://doi.org/10.1111/1750-3841.12380

Rahman, M. (2009). *Food properties handbook* (2nd ed.). CRC Press.

Sánchez-Romero, M. A., García-Coronado, P., Rivera-Bautista, C., González-García, R., Grajales-Lagunes, A., Abud-Archila, M., & Ruiz-Cabrera, M. A. (2021). Experimental data and predictive equation of the specific heat capacity of fruit juice model systems measured with differential scanning calorimetry. *Journal of Food Science*, *86*(5), 1946–1962. https://doi.org/10.1111/1750-3841.15693

Sulistyawati, I., Dekker, M., Verkerk, R., & Steenbekkers, B. (2020). Consumer preference for dried mango attributes: A conjoint study among Dutch, Chinese, and Indonesian consumers. *Journal of Food Science*, *85*, 3527–3535. https://doi.org/10.1111/1750-3841.15439

Sweat, V. E. (1974). Experimental values of thermal conductivity of selected fruits and vegetables. *Journal of Food Science*, *39*(6), 1080–1083. https://doi.org/10.1111/j.1365-2621.1974.tb07323.x

Talcott, S. T., Moore, J. P., Lounds-Singleton, A. J., & Percival, S. S. (2005). Ripening associated phytochemical changes in mangos (*Mangifera indica*) following thermal quarantine and low-temperature storage. *Journal of Food Science*, *70*(5), C337–C341. https://doi.org/10.1111/j.1365-2621.2005.tb09963.x

Zhu, X., Phinney, D. M., Paluri, S., & Heldman, D. R. (2018). Prediction of liquid specific heat capacity of food lipids. *Journal of Food Science*, *83*(4), 992–997. https://doi.org/10.1111/1750-3841.14089